Graphene Studies

Using Agilent Nanomeasurement Systems for Nanoscale Investigations of Graphene

Application Conspectus

Technology Advantages

- High-resolution atomic force microscopy (AFM) imaging capabilities
- Single-pass AFM Kelvin force microscopy mode (KFM) for easy and quantified probing of electrical properties
- Capacitance gradient (dC/dZ) imaging for sensitive detection of graphene and differentiation of various interlayer interactions
- AFM Scanning microwave microscopy mode (SMM) for surface impedance measurements
- Field-emission scanning electron microscopy (FE-SEM) for graphene multilayer domain identification and film defect detection

Data Examples

- High-resolution AFM imaging of graphene and graphene oxide (GO)
- Single-pass KFM and dC/dZ imaging of single-layer graphene (SLG) and few-layer graphene (FLG) on silica
- SMM studies of “white graphene”—hexagonal boron nitride
- Low-voltage FE-SEM imaging of graphene films on copper foil and nonconducting substrates

Overview

Graphene, a new member of the carbon family, has stimulated extensive interest in both academia and industry owing to its unique electrical, mechanical, and optical properties. With a monolayer of sp^2-bonded carbon atoms arranged in a honeycomb crystal lattice, graphene is a basic building block for all graphitic materials. Graphene-based nanoelectronics, in particular, are the subject of intense research.

Nanomeasurement systems from Agilent Technologies offer a broad range of novel atomic force microscopy and field-emission scanning electron microscopy methods, enabling researchers to study the properties of graphene at the nanoscale. Scientists in many diverse fields are authoring a steadily growing stream of published papers based on data obtained using Agilent’s innovative instrumentation and techniques. As well as affording revolutionary low-voltage FE-SEM capabilities, Agilent systems are now the most commonly utilized AFM solutions in the world for graphene research.

The material presented here merely hints at the scope of this dynamic and expansive body of data.

Agilent Technologies

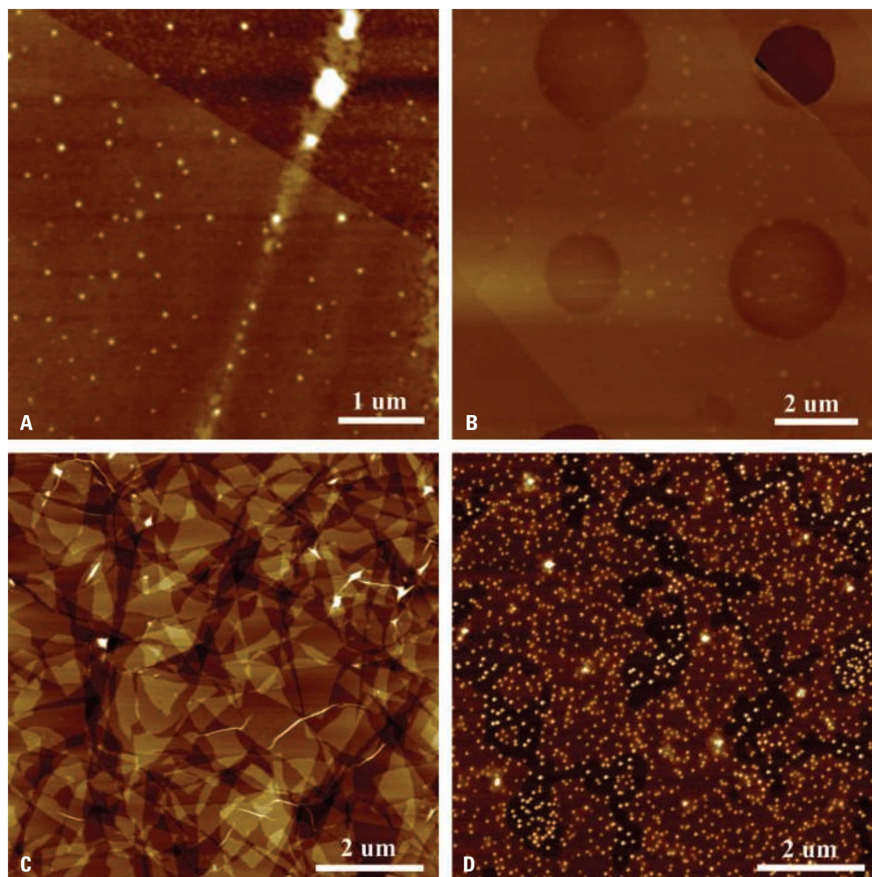

Figure 1. Examples of high-resolution AFM imaging of graphene and related nanomaterials. [A] Exfoliated SLG on silica. [B] Exfoliated FLG on a microfabricated silica substrate. [C] AFM imaging of single-layer graphene oxide nanosheets absorbed on a mica substrate. [D] AFM imaging of GO-silver nanoparticle composites.

High-Resolution AFM Imaging of Graphene and Related Nanomaterials

High-resolution visualization of surface morphology is a key feature of AFM. The ability to routinely resolve details at a single molecular level using an Agilent atomic force microscope has been well demonstrated previously.[1] A few examples of high-resolution AFM imaging of graphene and its derivatives are shown in Figure 1.[2,3]

Single-Pass KFM and Simultaneous dC/dZ Imaging Technique

The past two decades have witnessed a rapid growth of AFM and its evolution from a tool for merely acquiring a sample's morphology to one capable of probing additional materials properties. One good example is the development of the AFM imaging mode, single-pass KFM and simultaneous dC/dZ imaging technique via the introduction of a delicately designed triple lock-in amplifier (LIA) setup into the AFM electronics, i.e., the combined use

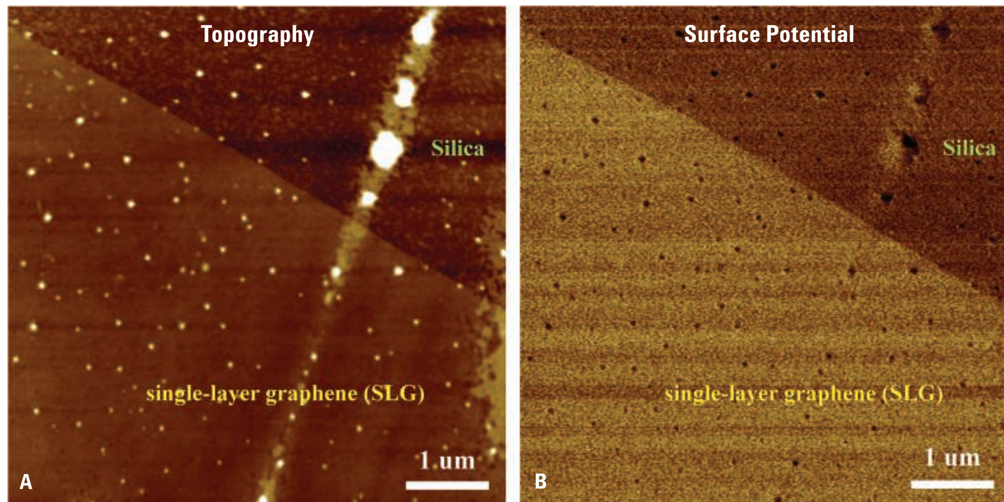

Figure 2. KFM imaging of single-layer graphene on silica. [A] High-resolution topographic image and [B] corresponding surface potential image.

of both the probe flexural resonance frequency ω_{mech} in the first LIA with a feedback loop for surface profiling, and a much lower frequency ω_{elec} in the second LIA with a second feedback control to null the tip/sample electrostatic interactions for quantitative measurements of sample surface potentials as well as its second harmonic $2\omega_{elec}$ in the third LIA to monitor the tip oscillation at this frequency caused by the electrostatic interactions for extraction of dC/dZ signal.

In contrast to the traditional KFM implemented via a two-pass approach known as lift mode, Agilent KFM is operated in the intermittent contact regime and the tip is always brought into the vicinity of the sample surface, thus significantly improving detection sensitivity and spatial resolution. More details about the principles and applications of this technique can be found elsewhere.[4,5]

Applications of KFM: Exploring Thickness-Dependent Electrical Properties of Graphene Materials

Much of graphene's appeal comes from its extraordinary electrical properties. Potential applications of graphene sheets as ultrathin transistors, sensors, and other nanoelectronic devices require them to be supported on an insulating substrate. Therefore, a quantitative understanding of charge exchange at the interface, as well as the spatial distribution of the charge carriers, is critical for device design. From this standpoint, Kelvin force microscopy offers an experimental means to investigate the local electrical properties of both SLG and FLG films. The effect of the film thickness on the surface potential is detected and quantitative measurements are obtained.

Single-layer graphene on silica can be readily identified by AFM. An example is shown in Figure 2A. The morphological difference between the graphene film and the substrate is easily observed. The graphene layer is much smoother, so individual granular features within the substrate area are resolved. Figure 2B is the corresponding surface potential image, in which the binary contrasts are captured and their boundary exactly matches the boundary between the two regions. This demonstrates that KFM can differentiate SLG from a substrate. Quantified measurement shows the surface potential variation between the two different materials is about 60 mV.[2]

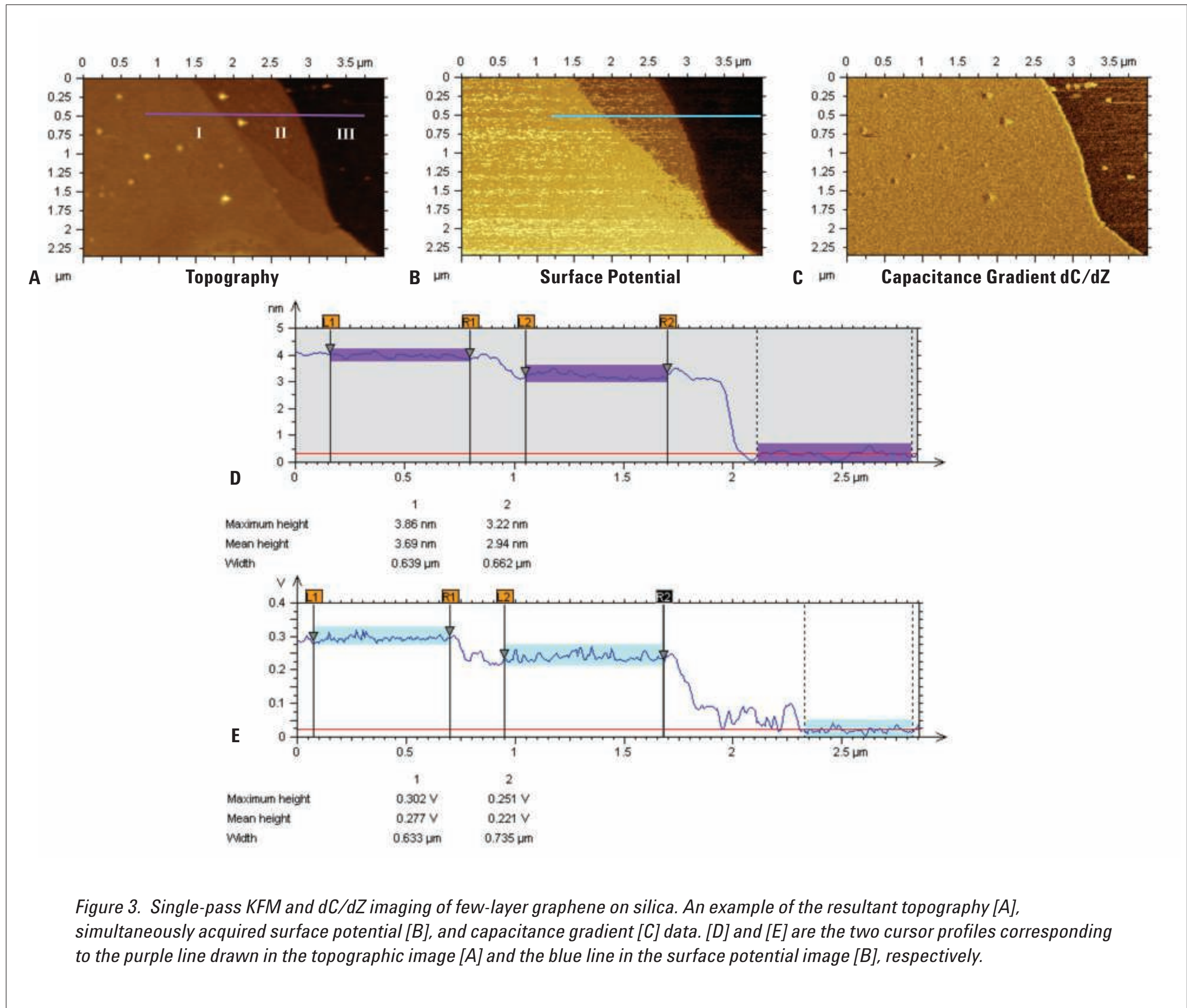

Figure 3. Single-pass KFM and dC/dZ imaging of few-layer graphene on silica. An example of the resultant topography [A], simultaneously acquired surface potential [B], and capacitance gradient [C] data. [D] and [E] are the two cursor profiles corresponding to the purple line drawn in the topographic image [A] and the blue line in the surface potential image [B], respectively.

Figure 3 shows single-pass KFM and dC/dZ imaging of FLG. Multiple steps are well resolved and three main regions (labeled as I, II, and III) are distinguished in the topography image, Figure 3A. Figure 3D is the cross-section profile corresponding to the purple line drawn in Figure 3A, from which region I can be derived to be about 0.75 nm higher than region II, as their apparent heights with respect to the bare substrate (region III) are 3.69 nm and 2.94 nm, respectively. The value, 0.75 nm, is in agreement with two times the highly ordered pyrolytic graphite (HOPG) interlayer spacing, 0.34 nm. This calculated bilayer change in film thickness is further confirmed by a well-defined single atomic step resolved between region I and region II in Figure 3A.

A layer-dependent behavior is detected unambiguously in the surface potential measurements. The thicker film in region I has a brighter contrast than that of region II in Figure 3B. The cross-section view of the blue line drawn in the surface potential image indicates that the variation of the surface potential between graphene film in region II (an eight-layer graphene film, based on its apparent height of 2.94 nm) and the silica substrate is about 221 mV, which is significantly higher than the 60 mV in the SLG example. The continued rise of two additional layers results in a further increase of 56 mV in region I with respect to region II.

In contrast to the thickness-dependent behavior seen in the surface potential data, both region I and region II, despite containing different graphene layers, exhibit a homogenous contrast that is brighter than that of the bare substrate in the dC/dZ image, Figure 3C. Such results can be validated by the fact that the dielectric constant of graphite material ($\varepsilon = 10–15$) is much higher than that of silica ($\varepsilon = 3.9$).

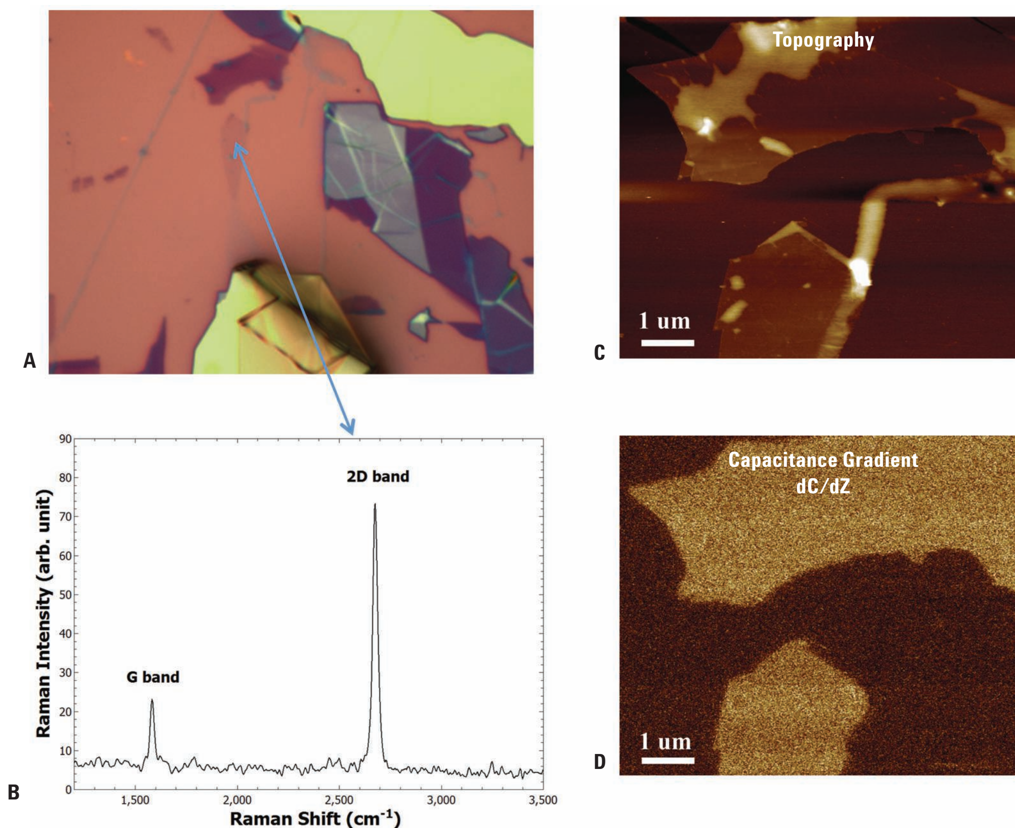

Figure 4. Ultrahigh sensitivity of dC/dZ imaging for detection of single-layer graphene. [A] An optical microscope image showing graphite flakes with various thicknesses on a silica substrate. [B] A Raman spectrum of the SLG at a location marked in the optical image. Both the AFM topography [C] and the corresponding capacitance gradient dC/dZ image [D] of that location.

Therefore, single-pass KFM and dC/dZ measurements allow the simultaneous monitoring of two distinctive properties that exhibit totally different behaviors in response to the graphene layer. This technique can be utilized to achieve a comprehensive characterization and gain a better understanding of graphene materials.

Applications of Capacitance Gradient dC/dZ Imaging: Sensitive Detection of Graphene and Differentiation of Various Interlayer Interactions

The promising observation that dC/dZ signals of typical FLG samples (thicker than five layers) are very distinctive from the substrate yet independent of the graphene layers provides motivation to conduct a systematic investigation of intensive and extensive applications of dC/dZ imaging for graphene characterization. A fundamental question is whether or not AFM-based capacitance gradient measurements have sufficient sensitivity to detect single-layer graphene, which is one of the thinnest materials in the world.

The ultrahigh sensitivity of dC/dZ imaging for detection of SLG is illustrated in Figure 4. Figure 4A is an optical photograph showing several graphite flakes prepared on a silica substrate. A specific region containing a small patch with the lightest optical contrast, i.e., the thinnest layer, is selected (marked by a blue line). A Raman spectrum, Figure 4B, of this location proves the two characteristic peaks, G band and 2D band. The intensity ratio of the 2D band over the G band is much higher than 1, and full width at half maximum (FWHM) of the 2D band is about 27 cm^{-1}, thus verifying it as an SLG film. In the dC/dZ image, Figure 4D, it is exciting to see that both this SLG film location as well as nearby FLG films at an upper location exhibit a much brighter contrast than the silica substrate.

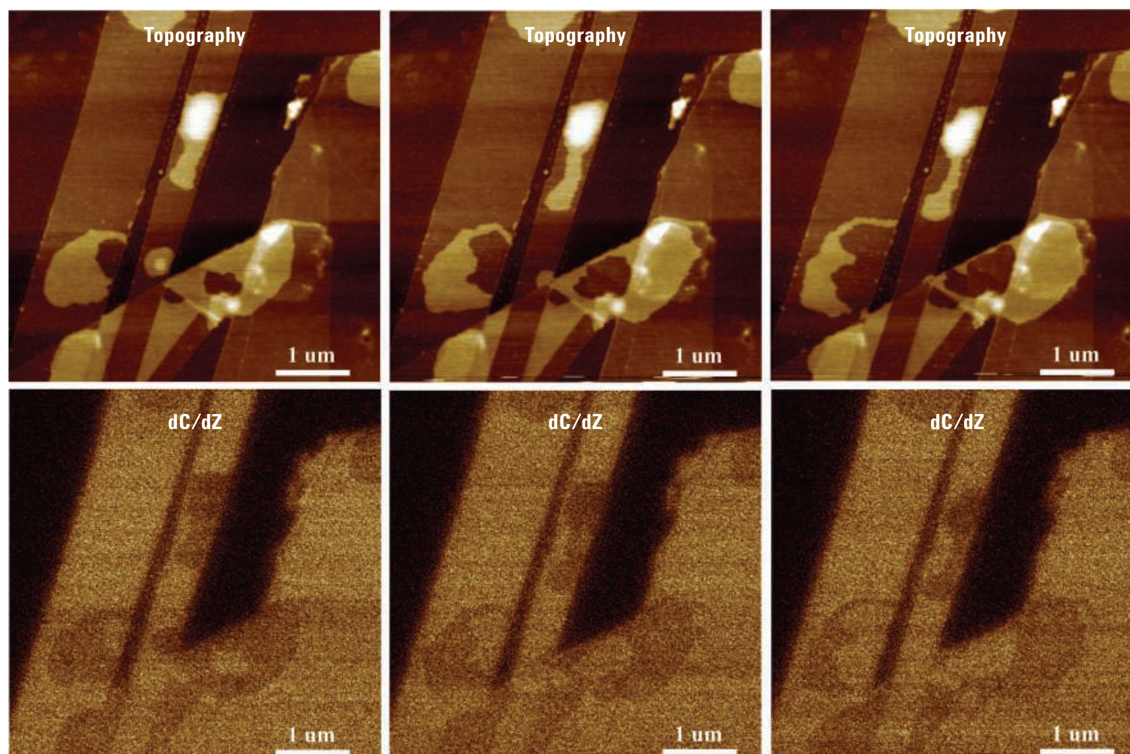

Figure 5. Detection of various interlayer interactions in FLG via dC/dZ measurements. [top row] Three selected in situ AFM topographic images showing the disturbance of some loosely bound small patches of graphene flakes by the AFM tip. [bottom row] The corresponding three dC/dZ images.

Figure 5 shows an exfoliated FLG sample with a few patches of graphene layer on top. These small patches are not attached to the underlying layers as firmly as the other regions, evidenced by the fact that they can be disturbed by the AFM tip at higher imaging force. The corresponding capacitance gradient images indicate that the dC/dZ signals at these locations are darker than at the surrounding FLG areas, strongly suggesting the potential application of dC/dZ imaging as an effective means to differentiate the interlayer interactions of the graphene flakes.

AFM Studies of Materials Beyond Graphene

One future direction of graphene-related research is to seek alternative layered inorganic materials as analogues of graphene — materials exhibiting some desired attributes that graphene lacks. Hexagonal boron nitride (h-BN), for example, attracts much attention because it is a III-V compound semiconductor with a wide band gap (more than 5 eV). The monolayer h-BN is often called “white graphene” and is predicted to be very useful as a complementary substrate for graphene electronics.

Figure 6A is a high-resolution topographic image of a few-layer h-BN synthesized via chemical vapor deposition (CVD). It exhibits a structural heterogeneity. Some regions corresponding to high-quality h-BN films are observed. Figure 6B is the close-up of one such location, indicated as a red square in Figure 6A. As can be seen, its surface morphology is both smooth and uniform; the quality is very close to those films produced using a mechanical exfoliation method. In addition, several protrusion islands corresponding to regions with one or more layers of BN are resolved.

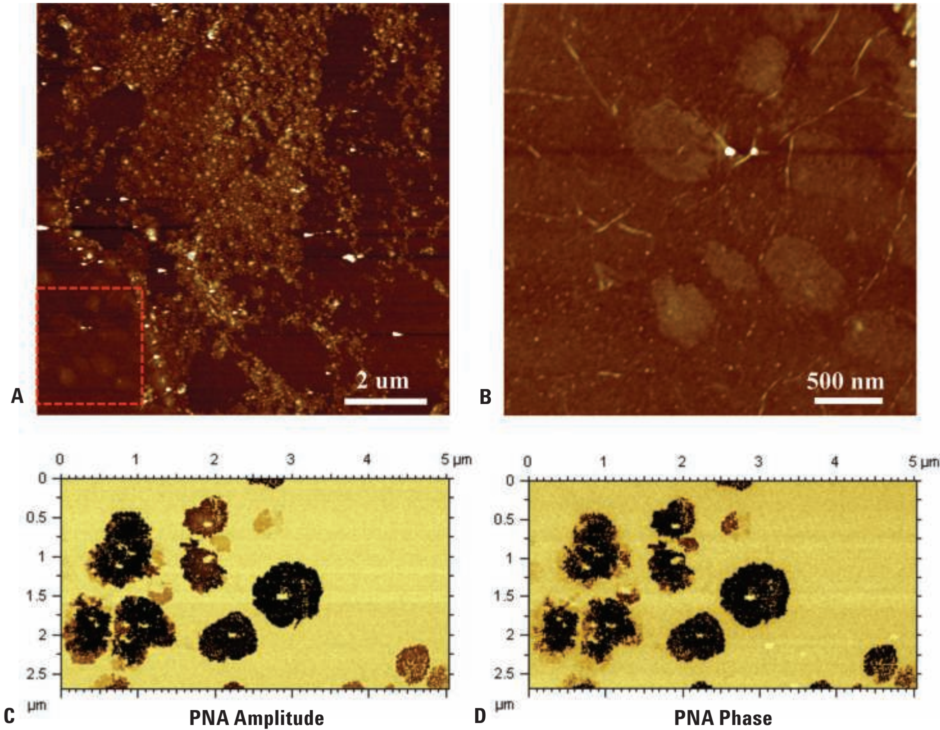

Figure 6. SMM studies of few-layer h-BN ultrathin films. [A] Topographic image revealing rich surface structures of few-layer h-BN ultrathin films. [B] A closer look at the high-quality h-BN location indicated by the red dotted square in [A]. The acquired PNA amplitude [C] and corresponding PNA phase [D] from SMM imaging of the same sample.

A recently developed, Agilent-exclusive technique known as scanning microwave microscopy is used to examine this h-BN sample. SMM utilizes an atomic force microscope interfaced with a performance network analyzer (PNA).[6] In the reflection mode (S11 measurement), the measured complex reflection coefficient of the microwave from the contact point directly correlates to the impedance of the sample under test.

The SMM results of the capacitance images (PNA amplitude and PNA phase) reveal that the double-layer films are fairly uniform across the region. Even though the existence of wrinkles caused by the materials transfer process or the grain boundaries of the underlying substrate is resolved in the topographic images, they are not clearly shown in the capacitance images. This indicates that the capacitance images are dominated by the film thickness and the dielectrics of the film.

It is interesting to see that the contrast variation (likely the capacitance difference) between the three-layer islands and the surrounding double-layer region are outstanding in Figures 6C and 6D. Since the difference in thickness between those layers is only about 1 nm, overall film thickness is about 3 nm. These results can be used to demonstrate the sensitivity of the SMM technique.

Low-Voltage FE-SEM Imaging of Graphene

Agilent's Nanomeasurement systems that utilize field-emission scanning electron microscopy to image graphene are also available. Agilent's innovative, miniature, all-electrostatic electron beam column

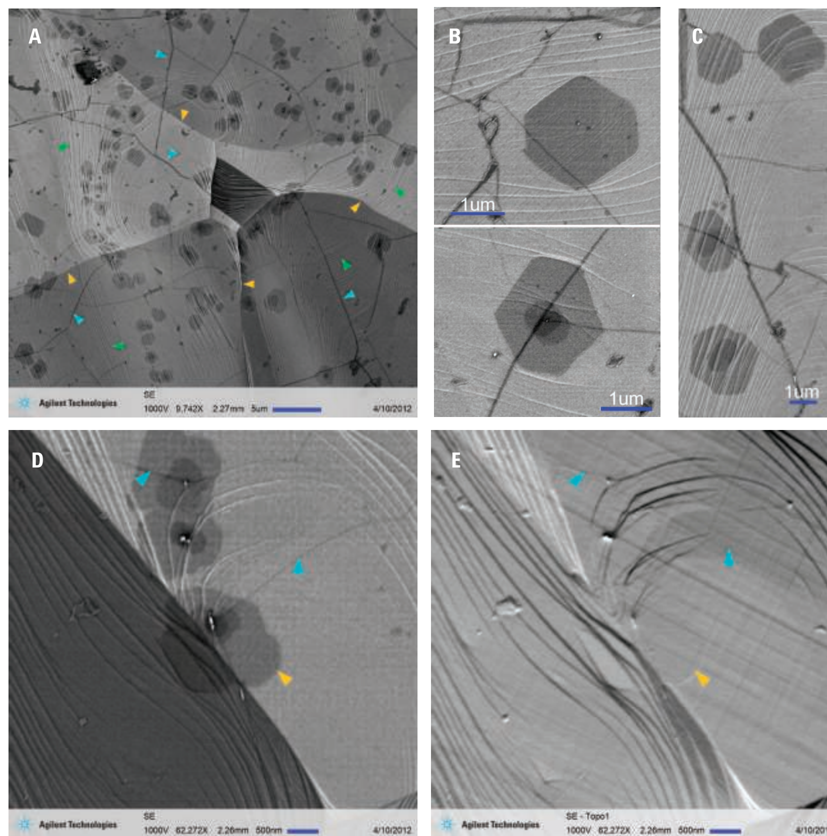

Figure 7. [A] Overview image of CVD graphene film on Cu foil showing features. [B] Some bilayer graphene domains showing a hexagonal shape. [C] All hexagonal domains show roughly the same orientation. [D] SE image at a high magnification. [E] Corresponding topo image giving topographic information.

design achieves high resolution at low beam voltages (500–2000V). In addition, a multichannel plate (MCP) electron detector that is sensitive to both secondary electrons (SEs) and backscattered electrons (BSEs) provides outstanding image quality with high contrast and excellent surface detail.

In Figure 7, low-voltage FE-SEM imaging of graphene deposited on copper foil via chemical vapor deposition is presented as an example of these capabilities.[7] Figure 7A shows typical features of the graphene film and the underlying Cu substrate. Both Cu grain boundaries (indicated by orange arrowheads) and Cu terracing with steps (indicated by green arrowheads) are apparent in the image. The dark lines (indicated by blue arrowheads) are characteristic graphene wrinkles that formed during the graphene film growth due to its thermal expansion mismatch with Cu.

The observation of graphene wrinkles crossing Cu boundaries and steps indicates the continuity of the graphene film all over the substrate, so the background in rather uniform brightness within individual Cu grains is actually the graphene monolayer. Another prominent feature is the darker flakes with a variety of shapes and dimensions that are attributed to multilayer graphene domains. A possible contrast mechanism in SEM images for different numbers of graphene layers has been described as the attenuation of secondary electrons from the substrate by graphene layers,[8] which is similar to the contrast formation in Auger electron spectroscopy.[9]

It can be seen in Figure 7A that most multilayer domains are not of a regular shape and some have a second, third, or fourth layer of smaller areas inside the domain. Nevertheless, a number of flakes can still be observed with some

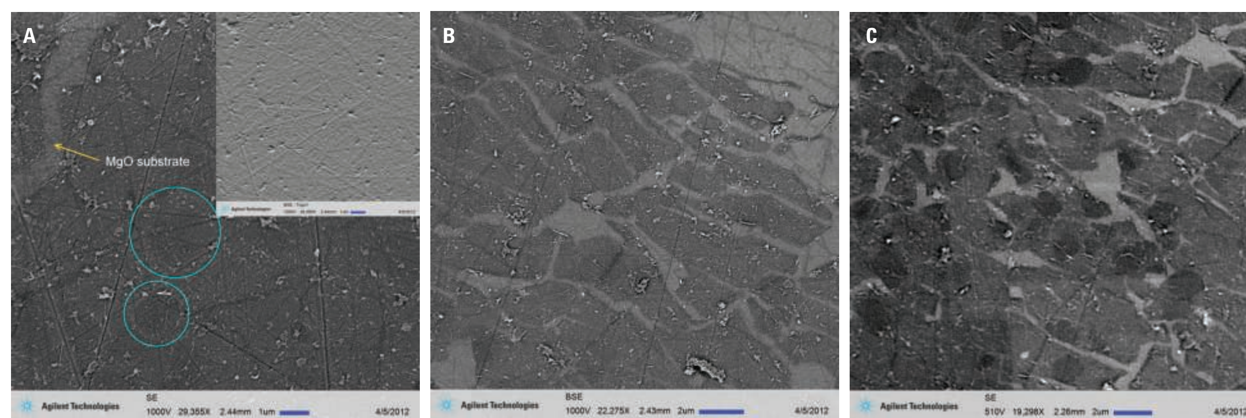

Figure 8. [A–C] Images of transferred graphene on a rough MgO substrate.

propensity towards six-fold domains. Figure 7B shows two domains in a regular hexagonal shape with well-identifiable 120° corners: one is a bilayer domain and the other one has bilayer, trilayer, and quadrilayer domains. A perfect graphene multilayer domain has the zigzag termination that was confirmed by Raman D band map.[10]

The formation of such hexagonal domains is associated with the etching role of hydrogen gas involved in the CVD process. Figure 7C reveals an interesting phenomenon: four hexagonal bilayer domains that have a roughly identical orientation within the same underlying graphene monolayer grain. This could be explained as the AB Bernal stacking of the bilayer graphene, where half of the carbon atoms in the second layer sit on top of the empty centers of hexagons in the first layer.[11]

Figures 7D and 7E present an SE image and its corresponding topo image at a high magnification, respectively. Compared to the SE image, the topo image reveals the Cu terrace more obviously due to its enhanced signal in the Z-direction. The narrow dark wrinkles (blue arrowheads), which consist of a couple of graphene layers, can still be discerned in the topo image, indicating the tiny height difference related to the graphene monolayer. The topo image can barely differentiate the multilayer domains, which are obvious in the SE image, from the monolayer. This is reasonable because the thickness difference of ~0.35 nm is beyond the capability of SEM. As indicated by the orange arrowhead, perceptibility of the bilayer edge in the topo image is most likely caused by the coincident edge of a Cu step and the bilayer graphene.

Low-voltage FE-SEM images of graphene films on three nonconducting substrates are presented in Figure 8.[7] For comparison, graphene films were transferred using the same technique. Figures 8A–8C are images of graphene transferred to an MgO substrate. A cracked area was located to show the contrast between the graphene film and the substrate. The area covered with graphene is darker in color than the bare MgO substrate, as shown in the left top area of Figure 8A.

It is not easy to differentiate multilayer domains (indicated by blue circles) on the graphene film. Apparently, the MgO substrate has a very rough surface and a large number of scratches. Unlike the SE image, the topo image (inset) does not display the edge of the graphene film. This can be explained as the topographic features of the graphene edge being overwhelmed by the rough MgO surface.

Figure 8B is a BSE image showing discontinuous graphene film on the MgO surface. BSE imaging can significantly reduce the charging because the high-energy backscattered electrons are less sensitive to charging than secondary electrons. Here, a similar resolution is obtained from BSE imaging. At low voltages, the electron beam generates a small interaction volume and the collected SEs and BSEs come from the same region in the sample. Hence BSE imaging at low voltages does not significantly affect the resolution. The SE image shown in Figure 8C was obtained using a beam of 510 V. No net charging was observed, and a better contrast from multilayer domains is seen.

In the case of graphene transferred to an Al_2O_3 substrate, charging

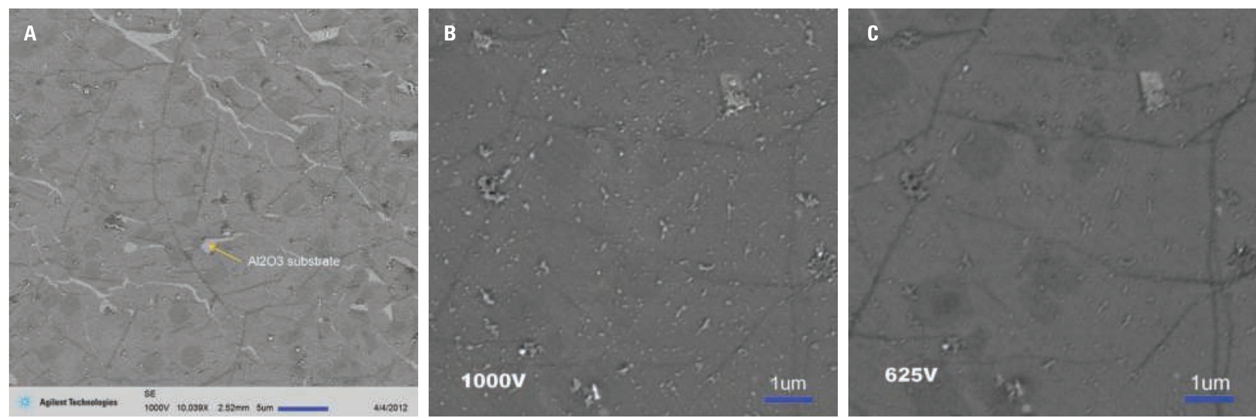

Figure 9. [A–C] Images of transferred graphene on an Al_2O_3 substrate.

was not observed at 1000 V. The transferred graphene film is smooth and multilayer domains are evident (Figure 9A). Compared to the image obtained at 1000 V (Figure 9B), the image obtained at 625 V (Figure 9C) displays the multilayer domains more obviously with an enhanced contrast. Figures 10A and 10B are an SE image and a BSE image of transferred graphene on an SiO_2/Si substrate, respectively. Graphene wrinkles can be seen in both images. Compared to the SE image, the BSE image displays a brighter SiO_2 substrate, which can be clearly explained as charge accumulation on the substrate surface. The image at a higher magnification (Figure 10C) not only reveals a corrugated morphology of the graphene film but also shows multilayer domains clearly, as indicated by a green circle.

Figures 8–10 reveal a remarkable difference in graphene morphology after transfer to different substrates by the same method. This preliminary study implies a distinct dependence of a graphene film's quality on the properties (e.g., surface roughness, hydrophilicity, crystallinity, and conductivity) of the substrate to which it is transferred.

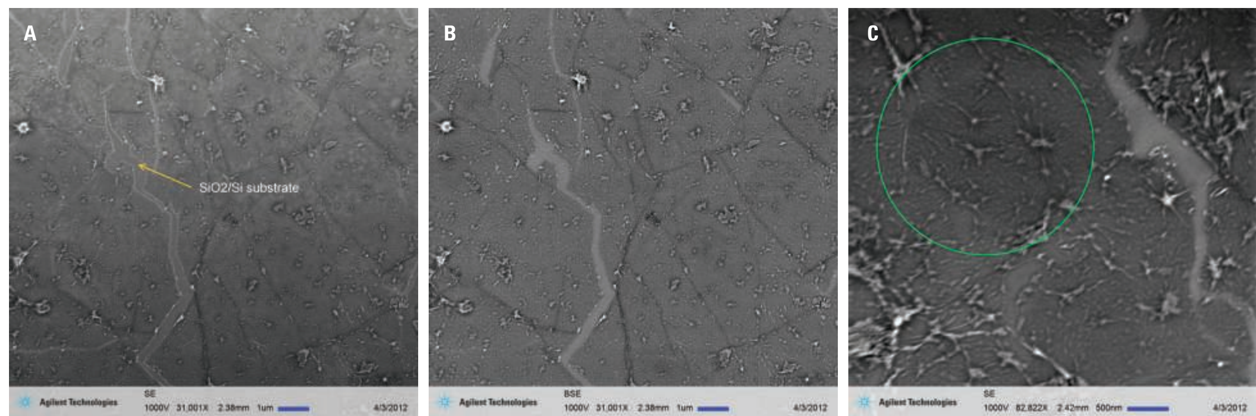

Figure 10. [A–C] Images of transferred graphene on an SiO_2/Si substrate.

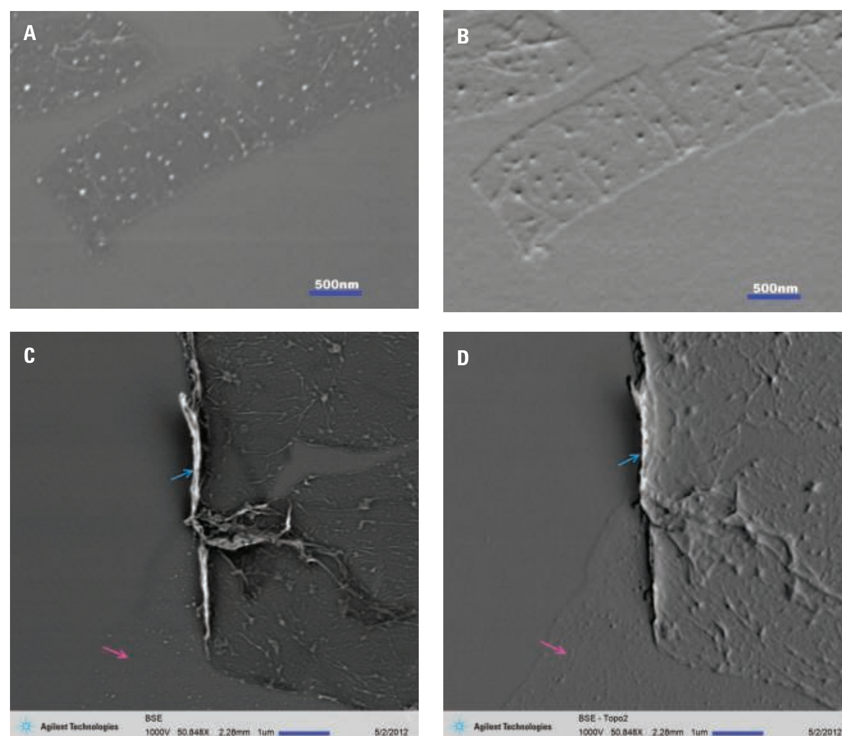

Figure 11. [A] SE image of a graphene ribbon showing nanoparticles on its surface; [B] topo image reveals more surface details; [C] SE image showing formation of a graphene nanoscroll at the edge of a film; [D] corresponding topo image of the nanoscroll.

Graphene films with special morphologies were also observed under the low-voltage FE-SEM. Figure 11A and 11B are SE and topo images of a graphene ribbon on a SiO_2/Si substrate, respectively. The ribbon shown here seems to have smooth and rather straight edges in parallel which possibly represent a well-defined zigzag or armchair structure. Bright spots on the graphene ribbon are likely impurity nanoparticles with 20–30 nm in diameter which were introduced during the transfer process. These nanoparticles are so bright in SE imaging that the graphene ribbon shows pretty weak relative contrast. The topo image which highlights topographical variations reveals enhanced surface details. From Figure 11B, even the folding history of the ribbon can be envisioned. The possible cracking of a graphene film along certain crystalline directions could cause the formation of such ribbon-like structures. The observed graphene ribbon here has an average width of ~1 µm which is much larger than that of previously reported graphene nanoribbons[13]. Nanoribbons with narrow widths (<~10 nm) are predicted to exhibit extraordinary electrical properties which are promising for high performance transistors working at room temperature.

An interesting carbon nanomaterial, a carbon nanoscroll, is a two-dimensional graphene sheet spirally wrapped into a tubular structure. The unique properties of carbon nanoscrolls include the $\pi-\pi$ interaction between the inner and outer walls, and electric current flowing within the scrolled graphene layer[14]. The intrinsic rippled structure of transferred graphene films on substrates are fragile and easily tear or crack. It was found that the edge of a highly corrugated graphene film always folds back and scrolls into a tubular structure[15]. One carbon nanoscroll (blue arrow) is shown in Figure 11C. The driving force for nanoscroll formation is the $\pi-\pi$ interaction of the overlapped parts which leads to a decreased total free energy of graphene[16]. In this case, the graphene film cracked due to the surface tension of water entrapped in the gaps between the graphene and the substrate in the drying process. After drying, the edge of the cracked graphene film became detached from the substrate and rolled up to from a carbon nanoscroll with a decreased total free energy. The pink arrow in Figure 11C indicates the polymer residue after the detachment of the graphene film. This residue is more obvious in the topo image, Figure 11D.

Acknowledgements

Samples for Figure 4 were kindly provided by Prof. Zexiang Shen of Nanyang Technological University (Singapore). Samples for Figures 1, 2, 3, 5, and 6 were generously provided by Columbia University (New York), Rice University (Texas), and University of Malaya (Malaysia). Dr. Ying Feng and Prof. Ke Chen at Temple University (Pennsylvania) kindly provided samples for Figures 7 through 10.

References

1. Yu *et al.* "Agilent 5600LS AFM High-Resolution Imaging: molecular-level understanding of n-alkane self-assembly onto graphite" *Application Note 5990-3956EN.* **2009,** Agilent Technologies, Inc.
2. Yu *et al.* "Thickness-Dependent Electrical Properties of Single-Layer Graphene and Few-Layer Graphene: a Kelvin force microscopy study" *Application Note 5991-0124EN.* **2012,** Agilent Technologies, Inc.
3. Yu *et al.* "Graphene Oxide and Its Applications Revealed by Atomic Force Microscopy" *Application Note 5991-0795EN.* **2012,** Agilent Technologies, Inc.
4. Magonov *et al.* "Advanced Atomic Force Microscopy: exploring measurements of local eclectic properties" *Application Note 5989-9740EN.* **2010,** Agilent Technologies, Inc.
5. Magonov *et al.* "Compositional Mapping of Materials with Single-Pass Kelvin Force Microscopy" *Application Note 5990-5480EN.* **2010,** Agilent Technologies, Inc.
6. Yu *et al.* "Microscopic Characterization of Few-Layer Hexogonal Boron Nitride: a promising analogue of graphene" *Application Note 5990-8893EN.* **2011,** Agilent Technologies, Inc.
7. Xie *et al.* "Imaging Graphene via Low-Voltage Field-Emission Scanning Electron Microscopy" *Application Note 5991-0781EN.* **2012,** Agilent Technologies, Inc.
8. W. Kochat, A.N. Pal, E.S. Sneha, A. Sampathkumar, A. Gairola, S.A. Chivashankar, S. Raghavan, and A. Ghosh, *Journal of Applied Physics* 110, 014315 (2011).
9. M. Xu, D. Fujita, J. Gao, and N. Hanagata, *ACS Nano* 4, 2937 (2010).
10. I. Vlassiouk, M. Regmi, P. Fulvio, S. Dai, P. Datskos, G. Eres, and S. Smirnov, *ACS Nano* 5, 6069 (2011).
11. K. Yan, H. Peng, Y. Zhou, H. Li, and Z. Liu, *Nano Letters* 11, 1106 (2011).
12. J.K. Hite, M.E. Twigg, J.L. Tedesco, A.L. Friedman, R.L. Myers-Ward, C.R. Eddy Jr., and D.K. Gaskill, *Nano Letters* 11, 1190 (2011).
13. X. Li, X. Wang, L. Zhang, S. Lee and H. Dai, *Science* 319, 1229 (2008).
14. X. Xie, L. Ju, X. Feng, Y. Sun, R. Zhou, K. Liu, S. Fan, Q. Li and K. Jiang, *Nano Letters* 9, 2565 (2009).
15. X. Liang, B.A. Sperling, I. Calizo, G. Cheng, C.A. Hacker, Q. Zhang, Y. Obeng, K. Yan, H. Peng, Q. Li, X. Zhu, H. Yuan, A.R. Hight Walker, Z. Liu, L. Peng and C.A. Richter, *ACS Nano* 5, 9144 (2011).
16. S.F. Braga, V.R. Coluci, S.B. Legoas, R. Giro, D.S. Galvao and R.H. Baughman, *Nano Letters* 4, 881 (2004).

AFM Instrumentation from Agilent Technologies

Agilent Technologies offers high-precision, modular AFM solutions for research, industry, and education. Exceptional worldwide support is provided by experienced application scientists and technical service personnel. Agilent's leading-edge R&D laboratories are dedicated to the timely introduction and optimization of innovative and easy-to-use AFM technologies.

www.agilent.com/find/afm

Americas

Canada	(877) 894 4414
Latin America	305 269 7500
United States	(800) 829 4444

Asia Pacific

Australia	1 800 629 485
China	800 810 0189
Hong Kong	800 938 693
India	1 800 112 929
Japan	0120 (421) 345
Korea	080 769 0800
Malaysia	1 800 888 848
Singapore	1 800 375 8100
Taiwan	0800 047 866
Thailand	1 800 226 008

Europe & Middle East

Austria	43 (0) 1 360 277 1571
Belgium	32 (0) 2 404 93 40
Denmark	45 70 13 15 15
Finland	358 (0) 10 855 2100
France	0825 010 700* *0.125 € / minute
Germany	49 (0) 7031 464 6333
Ireland	1890 924 204
Israel	972-3-9288-504/544
Italy	39 02 92 60 8484
Netherlands	31 (0) 20 547 2111
Spain	34 (91) 631 3300
Sweden	0200-88 22 55
Switzerland	0800 80 53 53
United Kingdom	44 (0) 118 9276201

Other European Countries:
www.agilent.com/find/contactus

Product specifications and descriptions in this document subject to change without notice.

© Agilent Technologies, Inc. 2013

Published in USA, September 17, 2013
5991-2068EN Rev.A

Agilent Technologies